Presented at the 51st Turbomachinery and Pump Symposium (2022)

A Comparative Study of Flooded and Directed-Lubrication Fluid-Film Thrust Bearings at High Load and Speed Conditions

Bruce Fabijonas
Research and Development Manager
Kingsbury, Inc.
Philadelphia, PA, USA

Richard Rodzwic
Research Engineer
Kingsbury, Inc.
Philadelphia, PA, USA

Bruce Fabijonas is Manager of Research and Development at Kingsbury, Inc. He oversees Kingsbury's suite of test rigs and is responsible for Kingsbury's bearing analysis software. He earned his PhD from the University of Illinois Chicago (Applied Mathematics, 1997) and is a member of STLE.

Richard Rodzwic is a Research Engineer at Kingsbury, Inc. He is responsible for testing focused on product development. He earned his MS from Philadelphia University in 2000.

ABSTRACT

Thrust bearings today are subjected to ever increasing speeds and loads while being constrained to fit in small footprints and to hold body temperatures to within API requirements. Consequently, bearing manufacturers are continuously searching for the next "super bearing" that meets customer demands. We present in this paper three different equalizing thrust bearing designs and their performance on a test stand. The first design is a traditional flooded bearing, and the remaining two designs are directed-lubrication bearings. All the bearings are lined with ASTM Grade 2 babbitt and have the same high (65%) pivot-offset to help them survive extreme test conditions. The bearings are subjected to load increments that terminate at alarm-triggering temperatures for several different shaft speeds. The tests show that one of the directed-lubrication designs is able to carry a higher bearing load than the other two designs while having a smaller bearing area at moderate to high speeds (206-345 fps (62.8-105.2 m/sec) at mean bearing diameter). We claim that this bearing design is a step towards meeting the above-stated customer demands. We perform preliminary computational fluid dynamic simulations to study the flow patterns in the designs with the hope of gaining insight into their cooling mechanisms. Finally, we demonstrate the difficulty of reproducing the individual bearing performances in terms of classical hot-oil-carryover theory.

INTRODUCTION

Fluid-film thrust bearings have been in use for over 100 years, yet they continue to be improved on a regular basis. The drivers for these improvements are the demands from the applications where these bearings are used. Examples include high-speed and high-load environments, the use of exotic lubricants, and the constraints of small footprints. Much to the chagrin of bearing manufacturers, the physical limits of the bearings remain unchanged. For example, those that use ASTM Grade 2 babbitt as the bearing lining must limit maximum film temperatures to 240°F (115°C) to avoid yielding of the babbitt lining. Many users, however, prefer a much lower operating limit to avoid thermal ratcheting or creep.

The basic theory of fluid-film bearing operation is straight-forward: oil between a stationary shoe and a rotating collar is dragged into

the gap between the two due to the adherence of the oil to both surfaces. As long as the gap between the two surfaces has a converging geometry, the squeezed oil creates a force that pushes up against the collar and carries the load. Simultaneously, the shearing of the oil within this gap generates heat. The oil that exits the bearing at the narrow end of the geometry is hotter than the oil entering the gap at the wide end of the geometry. A key task for a thrust bearing is to cool the hot oil exiting a pad before it enters the next pad. Many ideas have been suggested to disrupt the hot oil stream and/or increase the oil mixing between the pads. Popular methods place cool oil in proximity of or shoot cool oil at the rotating collar to which the hot oil adheres. These types of bearings are called directed-lubrication bearings.

Our goal with this paper is three-fold: first, we present recent results obtained on the high-speed test rig located at Kingsbury, Inc, using a relatively new design of a directed-lubrication thrust bearing and contrast these results against test data obtained on the same test rig in prior years using different bearing designs; second, we use Computational Fluid Dynamics (CFD) to gain insight into flow patterns and heat-transfer mechanisms in these bearings; finally, we demonstrate the challenge of using classical Hot Oil Carryover (HOC) theory in a Reynolds-equation based solver when trying to match the experimental data. In the remainder of this introduction section, we describe the three bearing designs considered as well as a few key features of the designs.

Design 1: Flooded Bearing

Conventional flooded tilt-pad thrust bearings as shown in Fig. 1 have changed little in design since the first days of Albert Kingsbury and George Michell. These bearings rely on natural mixing and convection in the space between pads as the oil cooling mechanism. In a series of papers, Gregory (1974, 1977, 1979) and collaborators (Capitao, et al. 1976) presented results of a detailed test campaign which studied the performance of a flooded 10.5 in (267 mm) thrust bearing in laminar and turbulent operating conditions; see also (Capitao 1976). This series of papers presented experimentally measured values of bearing power loss and pad temperatures under variable load, speed, and oil flow. Before the availability of fast bearing performance prediction software, these papers served as state-of-the-art tools for design engineers providing vital information about bearing performance.

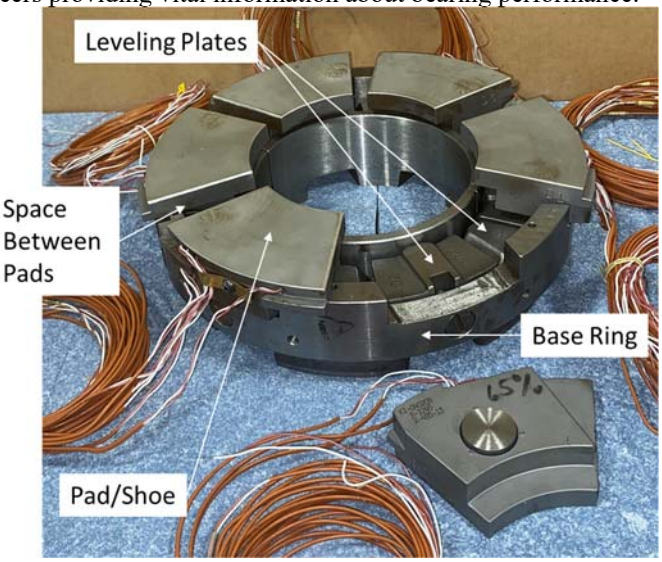

Figure 1: Flooded 65% offset steel bearing.

Design 2: Leading Edge Groove Bearing

The Leading Edge Groove (LEG®) thrust bearing, shown in Fig. 2, introduces cool oil at the leading edge of the pad by filling a groove located at that leading edge. A key feature of the LEG is that the groove rolls and pitches with the shoe. The design goal of the LEG was that it introduced cool oil directly into the hydrodynamic wedge between the pad and the HOC attached to the collar (Mikula and Gregory 1983). Later, it was conjectured that the design blocks the HOC (Brockwell, et al. 1994), though that argument has since been challenged (He 2003). Inserting oil directly at the leading edge of a pad is not a novel idea, e.g. see Bolton (1926), Firth (1933), and Lakey (1950). Mikula and Gregory (1983) introduced the current design of the LEG thrust bearing which Gregory (1985) subsequently patented. The design has the same load-carrying area as the traditional flooded design. The space between pads in the flooded design is now taken up by the groove on the leading edge of the pad in the LEG design, and very little room is left between the pads for conventional oil mixing; contrast Figs. 1 and 2. Mikula (1985, 1986, 1988a,b) described the benefits of the LEG thrust bearing by presenting data that showed that the LEG runs as good as or cooler than a conventional flooded thrust bearing with lower power loss. Wilkes and DeCamillo (2000) added a tapered region to the design downstream of the groove, thereby extending the range of speeds where the LEG can be used effectively. We emphasize that the design goal of the LEG was to fill the groove with cool oil and not to shoot cool oil at the collar like other directed-lubrication designs (e.g., spray bars).

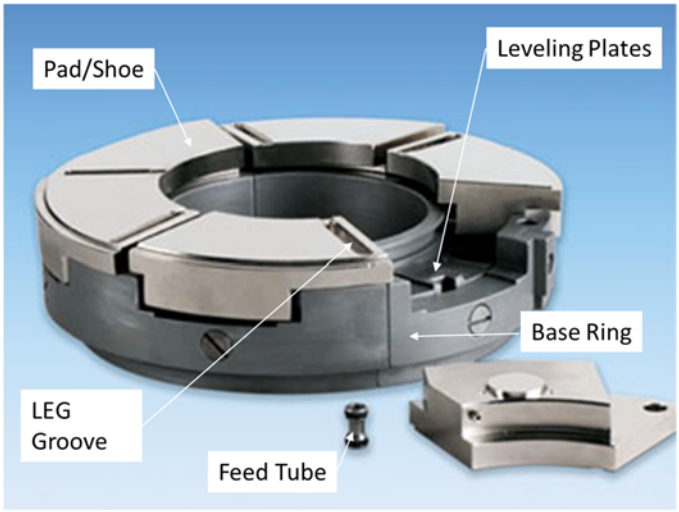

Figure 2: LEG 65% offset bearing.

Design 3: Between Pad Groove Bearing

The Between Pad Groove (BPG®) thrust bearing takes the design of a flooded bearing and adds troughs in the space between pads. These troughs are in proximity of the collar, fixed to the base ring (i.e., independent of shoe roll and pitch), and continuously filled with cool oil. The design philosophy is that the hot oil layer attached to the collar draws cool oil from the trough and mixes it with the oil in the hot layer. Placing such troughs in the space between pads is not a novel idea; see, for example, Ball and Gardner (1991), Ball (1996), and Ball and Byrne (1999). The design considered here, shown in Fig. 3, was conceived by DeCamillo (2005). A key feature of this design is the pads of the BPG subtend a smaller arc than those of a flooded design with identical inner and outer diameters. This allows the troughs to be wider than the space between pads in a flooded design, which in turn allow more "time" for the oil to cool between loaded surfaces. Like the LEG, the design goal is to fill the trough with cool oil rather than shoot oil at the rotating collar.

Figure 3: BPG 65% offset bearing.

Flooded vs. Evacuated Configurations

As the name suggests, a "flooded" configuration for thrust bearings is one in which the bearings and rotating collar are immersed in an oil bath. There are two common ways to achieve this in horizontal applications. The first way is to locate the oil drain in the housing at the top of the bearing cavity in a tangential orientation. The second way is to encase the outer diameters of the bearing and collar system using an oil control ring. The oil exits the top of the oil control ring tangentially into the thrust cavity of the housing. In

contrast, directed-lubrication bearings are set up in an "evacuated" configuration. In this scenario, the oil drains in the housing are located at the bottom of the bearing cavity, and the outer diameters of the bearings are not constrained. Oil exits the bearings into the housing cavity and flows down to the drains. In both configurations, the oil drains in the housing should be large enough to drain all the supplied oil. Although there are cases in the field in which a directed-lubrication bearing is run in a flooded configuration, or in which the drain capacity is less than the supply rate resulting in a pressurized thrust bearing cavity, they are not the norm. In the tests considered here, the flooded bearing was tested in a flooded configuration using oil control rings, and the directed-lubrication bearings were run in an evacuated configuration.

Equalizing vs. Non-Equalizing Thrust Bearings

Thrust bearings can either be "equalizing" or "non-equalizing." The difference between the two is whether the bearing contains leveling plates or not, respectively (see Figs. 1 and 2). These are components whose job is to keep the bearing face parallel to the collar. The common view is that they redistribute the load on a thrust bearing when the collar and the bearing face are misaligned (Koosha and San Andrés 2020). Although this does happen to some extent, the distribution is not perfect as demonstrated by Koosha and San Andrés and gets worse with misalignment angle. A more important task for the leveling plates is that they allow for variation in component stack-up height. The bearings tested here are equalizing.

EXPERIMENTAL SET UP AND RESULTS

Test Rig Description

The test rig on which these bearings were tested utilizes a horizontal shaft that tests two sets of double-acting thrust bearings simultaneously under load. It has been in active use since the early 1970s, is described fully in Wilkes, et al. (2000), and is schematically shown in Fig. 4. The test rig shaft is driven by a variable speed gas turbine with a rated output of 1100 horsepower (820 kW) and a controllable test speed range of 4,000 to 17,000 rpm. The turbine is connected to the test shaft through a gearbox by a flexible coupling. Two identical housings external to the turbine enclosure contain the bearing components. Two tilting-pad journal bearings at the extreme ends of the test rig support the test shaft.

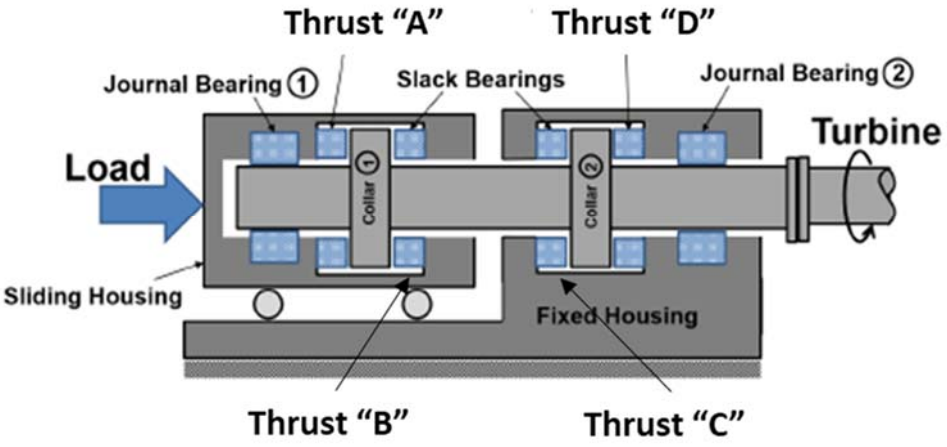

Figure 4: A schematic of the test rig (from San Andrés and Koosha (2018), with permission and modification).

Referring to Fig. 4, the "fixed housing" adjacent to the turbine is firmly secured to the foundation while the "sliding housing" is restrained but is free to slide axially on rails. An external hydraulic system applies an axial load to the sliding housing. As a result, thrust bearings "A" and "D" are loaded against each other while thrust bearings "B" and "C" remain unloaded (also known as slack bearings). The bearings are carefully shimmed to set the axial clearance, or end-play, of each double-acting thrust bearing. The flexible coupling between the test shaft and the gearbox is soft enough to absorb a large amount of axial shaft travel while exerting a negligible axial force on the gearbox.

Instrumentation

A data acquisition system records the test data. Steady-state measurements include shaft speed, applied thrust load, oil flow, oil supply pressures, oil supply temperatures, oil drain temperatures, and pad temperatures. Thermocouples with a range of 24°F - 1400°F (0°C - 760°C) and accuracy of 0.4% of reading measure the temperature data. A load cell with 50,000 lbf (222.4 kN) capacity and accuracy of ±0.15% of full scale measures the applied thrust load. Transient and steady-state data logs are recorded, where the transient log stores the data every second by averaging 120 samples per second and the steady-state log stores 30-second averages of the transient data. Finally, proximity probes monitor the position of various components within the test rig (e.g. the collar, the shaft, the housings). That data lies outside the scope of this paper.

Data Collection

During the start-up of the high-speed test rig, the shaft spins with a light load on the thrust bearings. The rotation speed is gradually increased to warm-up the supply oil reservoir and test fixture components. Once the temperatures reach the desired levels, the speed is adjusted to conduct the specific test, and the axial load is then increased at specified increments. Steady-state conditions are established by keeping the rotation speed, the bearing oil inlet temperature, the applied thrust load, and the oil flow rate to individual bearings to within ±50 rpm, ±1°F, ±5 psi, and ±0.2 gpm, respectively. Once these conditions are met at a given operating condition over a 30 second period, then the data is averaged for that period and recorded as the steady-state value.

Operating Conditions

Data from four independent test campaigns are presented here: one bearing of each design with steel-backed pads, and an additional BPG design with chrome-copper-backed pads. The operating conditions for the bearing under investigation in each campaign are given in the Table 1. We chose these tests so that the bearings are as similar as possible. All of the bearings are six-shoe, equalizing thrust bearings with a 10.5 in (266.7 mm) outer diameter (OD) and a 5.25 in (133.35 mm) inner diameter (ID).

Test Index	Test Bearing	Test Year	Bearing Area (in^2)	Bearing loads (psi)	Operating Speeds at Mean Diameter (rpm)	(fps)	Bearing Flow (gpm)
1	Steel Flooded	1997	55.2	150, 350, 500	5000	171.8	9.5
					7000	240.5	13.1
					9000	309.3	16.8
					11000	378.0	20.6
2	Steel LEG	2006	55.2	0, 150, 200, 300, 400, 500, 600, 700	6000	206.2	10.0
					8000	274.9	13.1
					10000	343.6	17.5
3	Steel BPG	2007	41.4	0, 200, 266, 400, 532, 600, 798	6000	206.2	10.0
					8000	274.9	13.3
					10000	343.6	17.5
4	Chrome Copper BPG	2017	41.4	0, 156, 313, 469, 626, 782, 939, 1095, 1174, 1252	6000	206.2	10.1
					8000	274.9	13.4
					10000	343.6	16.8

Table 1: Operating conditions for the four test campaigns.

The flooded and LEG designs have the same load-carrying area whereas the BPG design has a smaller pad angle to accommodate the troughs in the space between the pads. The remaining test conditions were uniform for the four campaigns: the oil type was ISO VG 32 and the oil inlet temperature was 120°F (48.9°C). These campaigns were conducted at different times over 20 years. Consequently, the speeds and flows do not line up between the tests exactly, but they are close enough for comparison here. Finally, all the bearings were tested in the "D" position (see Fig. 4).

Test Results

Given the different speeds listed in Table 1 between the flooded bearing and the other bearings, pad temperatures for the flooded bearing were interpolated to the speeds of the directed-lubrication bearing tests; see Appendix A. Figures 5-7 show the test results for all bearings as a function of bearing load for various shaft speeds. It is necessary to keep in mind the fact that the area of the BPG design is 75% that of the LEG and flooded designs. However, the oil flow rates are almost the same for all the bearings. Tests for a given speed were terminated when 75/75 temperatures reached the 240°F (115°C) temperature limit or the loading applicator on the test rig reached its maximum.

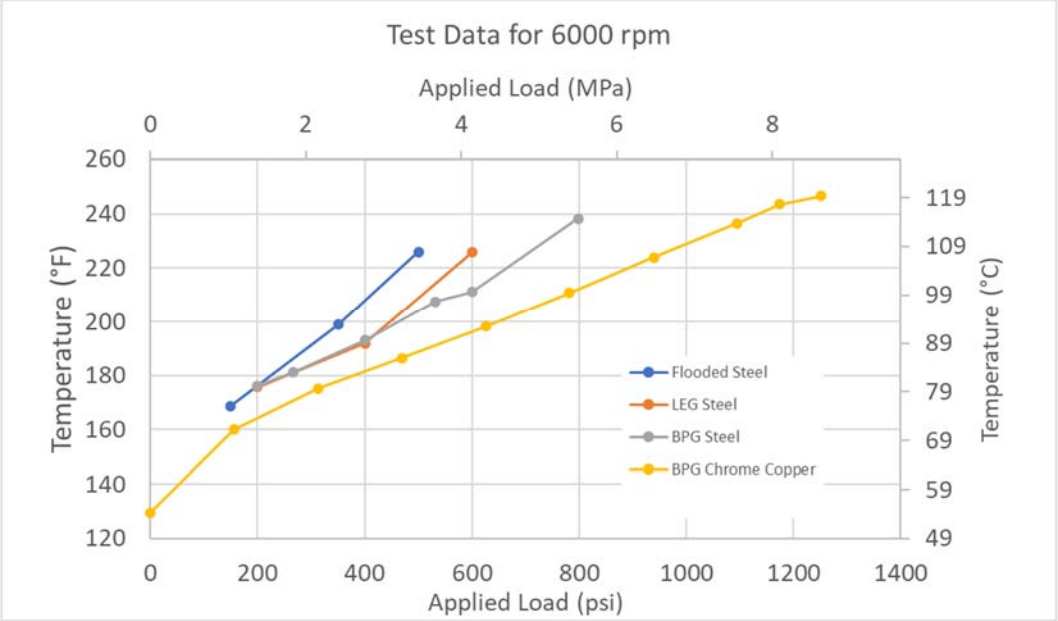

Figure 5: Pad temperature measured at the 75/75 location at 6000 rpm.

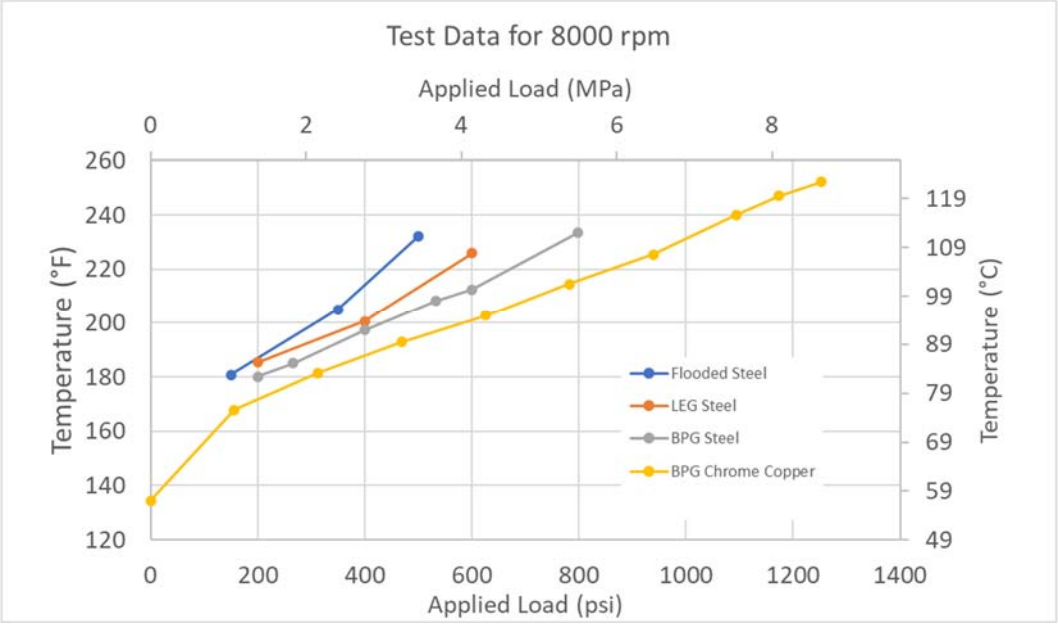

Figure 6: Pad temperature measured at the 75/75 location at 8000 rpm.

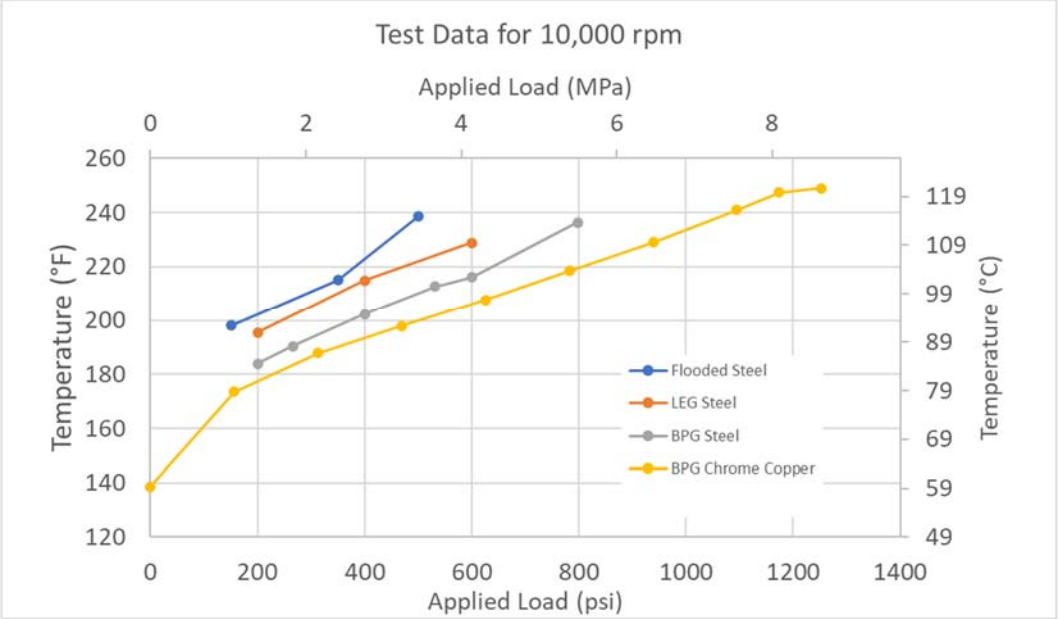

Figure 7: Pad temperature measured at the 75/75 location at 10,000 rpm.

There are several takeaways from Figs. 5-7:

1. In all cases tested, the chrome-copper BPG runs cooler than the other bearings when viewed in terms of bearing load.
2. The steel BPG outperforms the flooded and LEG counterparts.
3. The cooler temperatures of the chrome-copper BPG allow it to be loaded up to 1252 psi load at all speeds tested. (This corresponds to the test rig's load capability.) None of the other bearings were able to attain such a high load before reaching the 240°F operating limit. The bearing did this with a smaller bearing area than the LEG and flooded designs.

The conclusion we draw is that a BPG-design bearing can meet, if not beat, the performance of a flooded- or LEG-design bearing *with a larger footprint*. We present an example in the next subsection.

An example of the BPG smaller footprint

The challenge in sizing a thrust bearing is to maximize the bearing area (which decreases the bearing load) while minimizing the collar surface speed (which lowers pad temperatures). Consider a request for a thrust bearing that could withstand a moderate load (17,221 lbf) at a fast shaft speed (14,250 rpm) with a minimum ID (8.65 in (224.8 mm)). The combination of high speed and moderate load made bearing selection difficult. The traditional recommendation was for a 10-shoe, 12-in LEG with a 65% offset. Unfortunately, the predicted 75/75 temperatures exceeded the 240°F (115°C) temperature limit. The LEG design was limited by the oil flow rate through the bearing. A 10-shoe, 12-in chrome-copper BPG, shown in Fig. 8, was built and tested. The bearing has an area of 32.4 in^2 (20,903 mm^2), a smaller pad angle than a traditional LEG, tapers on the leading edges, and a 68% pivot offset.

Figure 8: 10-shoe BPG thrust bearing.

A careful examination of Fig.8 shows two supply holes feeding the trough. The high surface speeds required a high flow volume to keep the bearing cool. The bearing design allowed for a second supply path to be machined into the base ring from the supply annulus to each of the troughs. The operating conditions for the test of this bearing are given in Table 2, and a graph of its performance is shown in Fig. 9. We see that at 14,000 rpm, the bearing temperature is below the 240°F (115°C) limit for loads less than 38,800 lbf (172 kN) with an oil supply rate of 55 gpm (208.5 l/min).

Operating Speeds at Mean Diameter			Oil Supply Flow	
(rpm)	(fps)	(m/s)	(gpm)	(l/min)
6000	272.9	83.2	23	87.2
8000	363.9	110.6	30	113.7
10000	454.9	138.7	38	144
12000	545.9	166.4	47	178.1
14000	636.8	194.1	55	208.5

Table 2: Operating conditions for the BPG thrust bearing shown in Fig. 8.

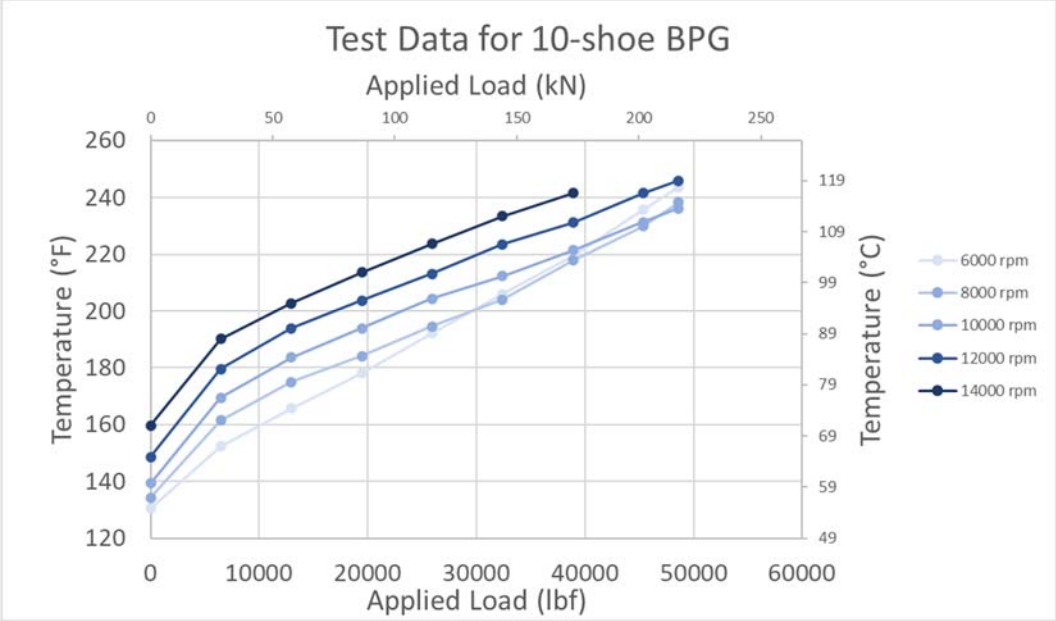

Figure 9: Pad temperature measured at the 75/75 location for the 12-in 10-shoe BPG thrust bearing for the flows in Table 2.

The takeaway is that the proposed BPG was able to maintain a small footprint and deliver a large amount of oil to limit pad temperatures.

COMPUTATIONAL RESULTS

The problem with numerical simulation of bearing performance using CFD has always been a matter of scale. Film thickness, crucial to the entire theory, is on the order of thousandths of an inch, whereas scales in the orthogonal directions vary from inches to hundreds of inches, a variation of three to six decades of length scale. Neither the CFD solvers nor the computer architecture of the 20th century were equipped to tackle this problem. Consequently, the bearing community took a different approach. The codes developed at the end of that century, known as thermo-elasto-hydrodynamic (TEHD) solvers,

- solve the simpler two-dimensional Reynolds equation for pressure on the shoe surface rather the three-dimensional Navier-Stokes equations in the entire fluid domain;
- solve the three-dimensional energy equation in the fluid region between the thrust shoe and the runner;
- solve for the mechanical deflection of the shoe and/or runner;
- model the physics that occurs in the space between pads (referred to collectively as HOC models).

The HOC models blend the hot oil leaving the trailing edge of pad with cool oil in the space between pads to form a boundary condition for the oil temperature at the leading edge of the pad. Often, these models contain free parameters to help match computed results with test data. Gates (2019) provides an excellent summary of popular mixing models. Yang and Palazzolo (2021a,b) describe challenges with such models and summarize their weaknesses.

Advancements in computer technology and software in the 21st century now allow for bearing analysis using CFD. The breadth of CFD simulations carried out in the last 20 years makes it impossible to identify all the truly groundbreaking CFD work. That said, some noteworthy examples include the work of Pajączkowski (2010) and, most recently, Yang and Palazzolo (2019a,b, 2021a,b,

2022a,b). The former author showed that commercially available CFD software has matured enough to analyze thrust bearing performance in both steady-state and transient, and the latter pair of authors showed that the software can compute advanced topics like dynamic coefficients and can be used to study intricate models whose physics remains unclear (the Morton Effect). Although these works are resource intensive, they show that commercially available CFD packages are capable of predicting bearing performance.

CFD Analysis

Problem Setup

The results presented in this section come from preliminary CFD calculations conducted using ANSYS CFX for the operating conditions in Table 3.

Applied Load	291 psi (2 MPa)
Shaft Speed	10,000 rpm
Oil Type	ISO VG 32
Oil Supply Temperature	120°F (48.9°C)

Table 3: Operating condition for numerical simulations.

Each of the CFD models focuses on only one sixth of the full bearing model and employs rotational symmetry. We use the Walther model for viscosity dependence on temperature (Seeton 2006) for ISO VG 32:

$$\ln[\ln(\nu + 0.7)] = -3.66608 \ln(T/436.9470).$$

Here, T is temperature measured in Kelvin and ν is the kinematic viscosity in centistokes. Density as a function of temperature for ISO VG 32 oil is given by

$$\rho(T') = 889.5 - 0.6097\, T',$$

where ρ has units of kilograms per cubic meter and T' is in degrees Celsius (DeCamillo and Fabijonas 2012). We turn on the full thermal energy model within the CFD solver with viscous dissipation but use adiabatic boundary conditions at the fluid-solid interfaces for the sake of simplicity. The shoes in the models are allowed to roll and pitch with operating conditions. The film thickness and pitch and roll angles in each case are determined using an optimization or a Newton-Raphson scheme. The criteria are that the computed load matches the applied load to within some tolerance and the pad moments of inertia induced by the pressure field are small. We allow for turbulence in the oil using the shear stress transport (SST) model. The supplied oil flow converted to a mass flow rate serves as the inlet boundary condition, assuming the flow is equally distributed among the six pads. The moments imposed by the pressure field on the shoe are computed by importing the pressure field into ANSYS MECHANICAL. We fix a small circle on the shoe support as the contact surface between the pad and the leveling plate and compute the moments about that fixed circle, the diameter of which is computed using Hertzian sphere-on-flat-contact calculations.

Figure 10 shows CAD models of the three bearings considered here. Note that all chamfers, fillets, screws, and anti-rotation keys have been removed to simplify the meshing process. The flooded and LEG bearings have a non-load-carrying lip on the OD of the pad and a large undercut on the leading edge. In contrast, the BPG has no lip on the pad OD and no undercuts. In each analysis, the CAD model shown in Fig. 10 is imported into the geometry engine of the CFD software. The bearing is artificially enclosed by a solid body. Finally, the bearing "cuts" the enclosing solid body, and what is left is the fluid that surrounds the bearing. The 1/6th sub-models created this way are seen in Figs. 12, 17, and 22 below.

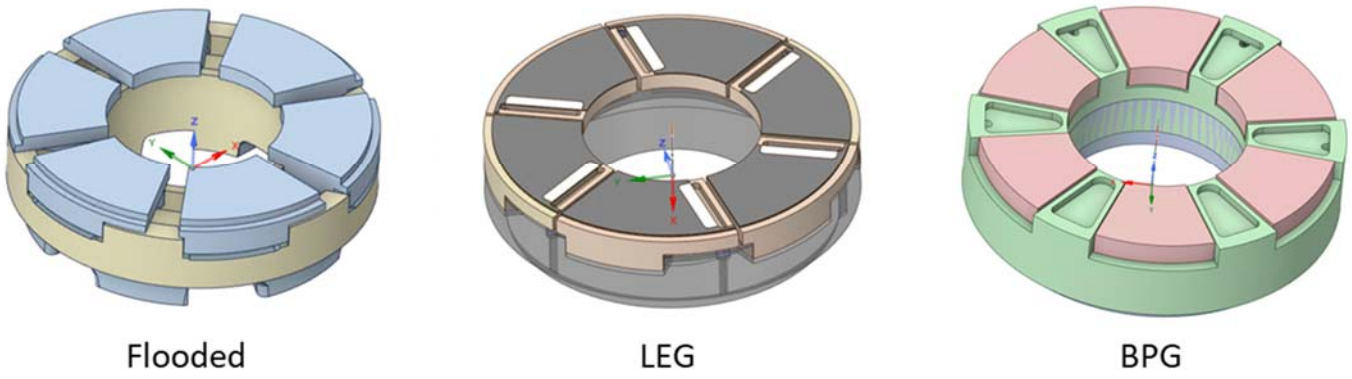

Figure 10: CAD drawings of all three bearings considered here.

Streamlines

The goal of these simulations is to study the streamlines of the velocity field and how they mix for each bearing type. In general, there is a difference between streamlines, streaklines, and pathlines (or flowlines). However, in steady-state flows as considered here, these are all the same, so we focus on the streamlines generated by the CFD post-processing software.

Views of the streamlines are challenging, though state-of-the-art CFD software allows for great flexibility in choosing which streamlines to study. A particularly useful feature is that a user can "seed" streamlines on a specific surface. This means that the CFD post-processing package can generate streamlines that start or stop at a particular surface. For example, a user can seed streamlines in the film layer at the trailing edge of the pad and see how it mixes with the fluid in the space in between the pads.

In the figures below, streamlines are colored by oil temperature with blue being the supply temperature and red being the hottest computed temperature. These temperatures are representative and should not be used to compare with measured test data. The adiabatic fluid-solid boundary condition used in these simulations is a first-pass attempt at understanding the effects of the different supply methods. A full analysis needs to include heat conduction into the solids as well as pad deflection. It is anticipated that future work will include these effects.

Design 1: Flooded Bearing

Referring to the left bearing in Fig. 10, the base ring of a flooded bearing (in beige) has "feet" on the bottom. Oil is supplied to the bearings in the test rig at a fixed rate to the space behind the base ring. Since the volume is enclosed, the oil flows from behind the bearing, along the rotating shaft, and finally over and around the shoe body. The oil exists the OD of the thrust bearings and is captured at the collar OD by oil control rings (not pictured or directly modeled).

We create our $1/6^{th}$ sub-model of the full bearing by slicing approximately mid-way in the space between pads. The slicing choice allows the shoes to roll and pitch while remaining in the enclosed fluid envelope. Furthermore, the fluid region extends beyond the OD of the pad, again to allow the pad to pitch and roll while remaining fully within the fluid region. Figure 11 graphically shows the boundary conditions used in the CFD simulation: the black arrows show the oil supply region; the blue arrows show the "opening" boundary condition near the pad OD; the purple arrows indicate regions where rotational symmetry is employed; and the small green arrows indicate the interfaces between different regions. The opening boundary condition near the pad OD allows for oil to flow in both directions across the boundary, thus simulating a flooded environment. The temperature of the oil that may enter the OD is set as 183°F (84°C), which is the temperature measured in the drain located in the housing at the operating condition in Table 3. Additionally, the shaft and top surfaces are fixed walls rotating at 10,000 rpm, and the remainder of the exterior surfaces are fixed walls.

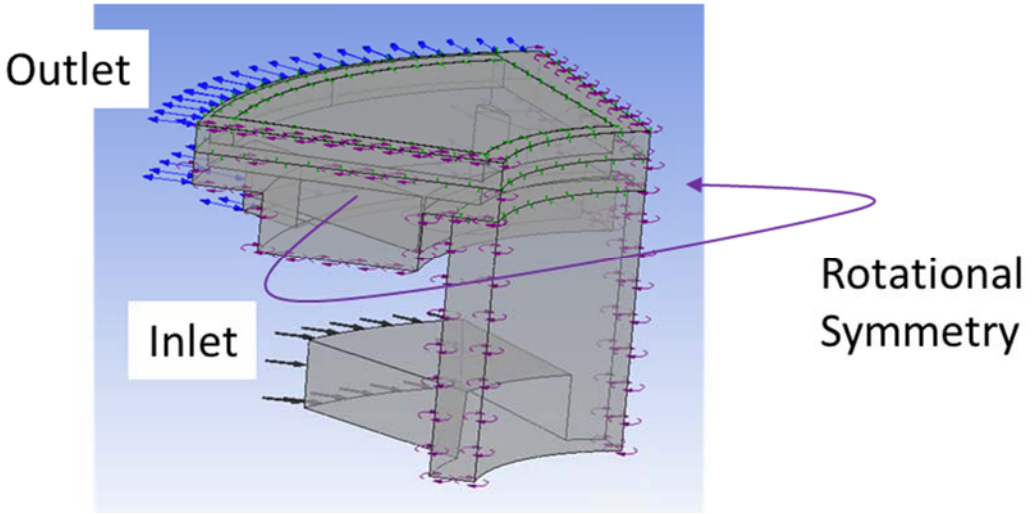

Figure 11: Boundary conditions used in the fluid domain for the flooded bearing.

Axially, the region is divided into three layers illustrated in Fig. 12: the film layer is defined by the loaded and runner surfaces, the second layer is defined by the lip at the OD of the pad and the film layer, and the third layer is the rest of the fluid. The two top layers are meshed using the CFD solver's "sweep" method in the axial direction. The method allows the user make copies of a surface mesh in a direction perpendicular to the surface as many times as desired. Although very powerful, the method requires that the target surface (the terminal surface generated by the method) be a projection of the source surface, i.e. the two surfaces must be isomorphic. This requirement forces us to separate the film layer into two regions: one is over the shoe (green region in Fig. 12), and the second is over the enclosing fluid (grey region in Fig. 12). These regions are propagated through the layers when possible. That is to say, the green region in Fig. 12 exists only in the film layer and not the second or third layers since there is no fluid region in those layers. The mesh is "refined" along all fixed walls to account for shear between the fluid and the zero-velocity walls, and that refinement is carried through all axial layers. A picture of the meshed shoe, including a close up, is seen in Fig. 12.

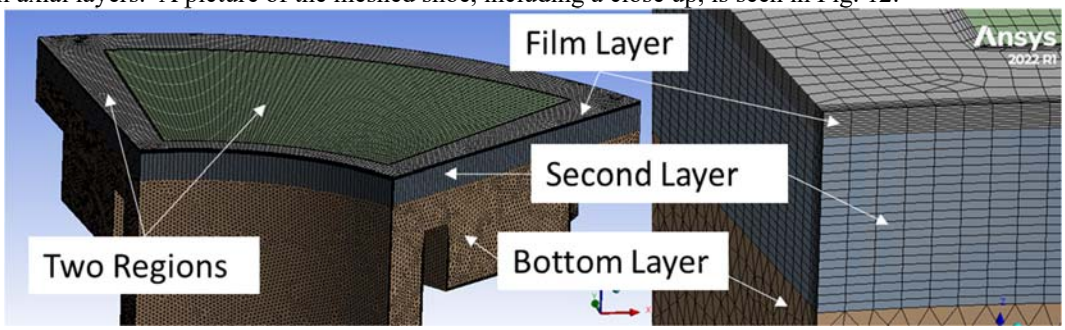

Figure 12: View of the mesh of the flooded bearing used in the CFD solver, the three different layers, and the two regions in each layer.

Figure 13(a) shows the computed pressure field on the loaded surface generated by the rotating collar.

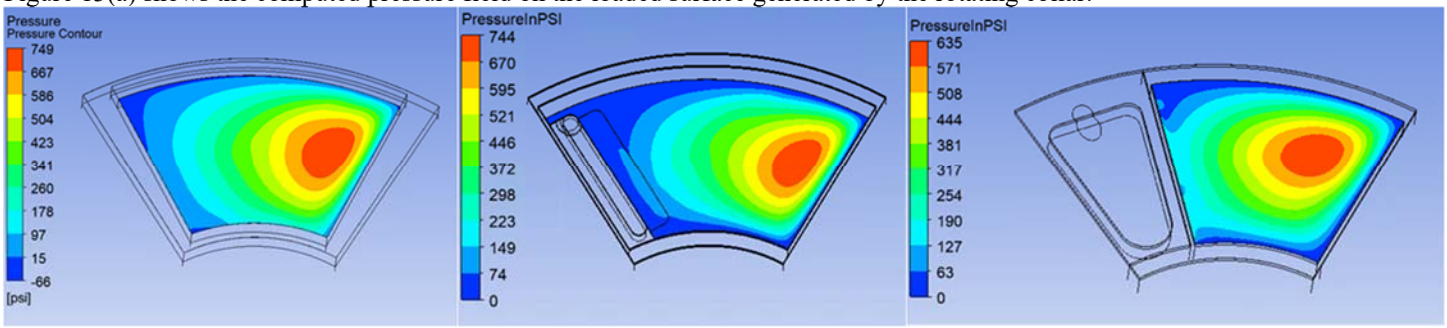

Figure 13: Pressure field computed by the CFD program for all three bearing designs. Shaft rotation in each picture is clockwise.

Figure 14 shows the streamlines seeded at the trailing edge of the film layer in the region above the pad. Much of the oil remains in the layer with a trend to flow towards the OD. The temperature increases radially, and very little cooling takes place across the space between pads. Figure 15 shows the streamlines seeded at the interfaces of the layers. They suggest that oil in the second layer enters

the film and vice versa. In contrast, oil that surrounds the pad in the bottom layer for the most part does not enter the film.

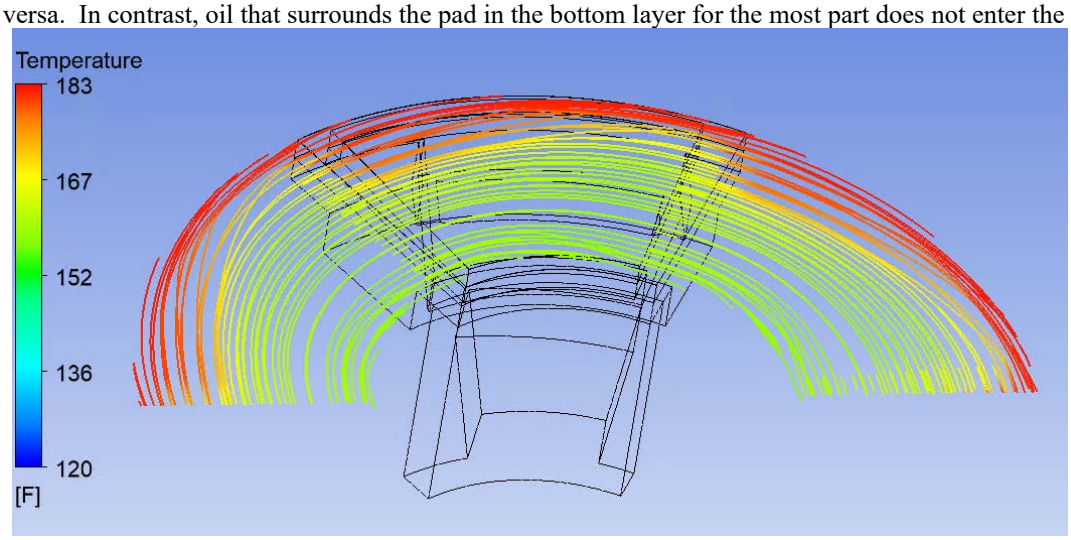

Figure 14: Streamlines for the flooded bearing seeded at the trailing edge of the loaded region in the film layer. The pattern has been repeated to get a better grasp of the streamlines. Shaft rotation is clockwise.

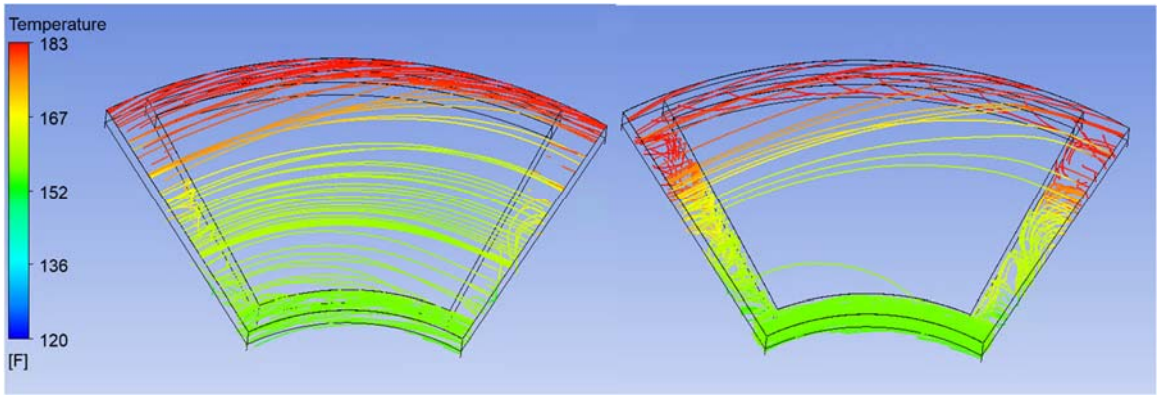

Figure 15: Streamlines for the flooded bearing seeded at the interfaces of the film and second layers (left) and second and bottom layers (right) (refer to Fig. 12). Shaft rotation is clockwise.

Design 2: LEG Bearing

Early CFD work on LEG journal bearings (Edney, et al., 1998) studied a 2D slice through the centerline of an LEG journal bearing. Their work used pad tilt angles determined by a Reynolds-equation based solver. The goal of that work was to numerically evaluate the effect of a taper added to the trailing edge of the groove. Their paper demonstrated that a recirculation zone exists within the groove and that the zone affects the oil temperature at the leading edge of the pad. They showed that the addition of the taper removed a step change in pressure at the leading edge of the pad and moved the peak pressure downstream on the pad. They concluded that the taper promotes hydrodynamic pressure generation on the pad.

The middle bearing in Fig. 10 shows the model of the LEG shoe. The steel body is shown in beige and the loaded surface is shown in gray. Two features are worth pointing out: first, the babbitt in front of the groove (referred to as the leading-edge strip) has been removed; second, there is a taper in the babbitt layer behind the groove shown in white, and that taper meets the groove above the steel body. Finally, the oil supply mechanism is dramatically different for the LEG than the flooded bearing. In the LEG, oil is supplied to an annulus in the OD of the back of the base ring. Feed paths from the annulus to the leading edge of the pad are machined into the base ring. The oil exits the feed path at the surface of the pad, fills the groove, and ultimately exits the system at the OD of the collar.

As we did for the flooded bearing, we create our $1/6^{th}$ sub-model of the full bearing by cutting the domain in the space between pads. Figure 16 graphically shows the boundary conditions used in the CFD simulation of the LEG thrust bearing. The colored arrows are exactly as described for Fig. 11. There are two key differences from the flooded bearing model. First is the omission of a fluid cavity behind the bearing. This is a consequence of the different feeding mechanism for the LEG. Second, the fluid domain is a two-fluid region, a mixture of oil and air. The inlet condition is oil only, and the opening boundary condition near the pad OD allows air and oil to flow out through the boundary but only air to flow in, thereby simulating the evacuated environment. The temperature of the air at the inlet is fixed at XXX, which corresponds to the temperature of the oil at the drain at the bottom of the thrust bearing cavity in the housing for the operating condition in Table 3.

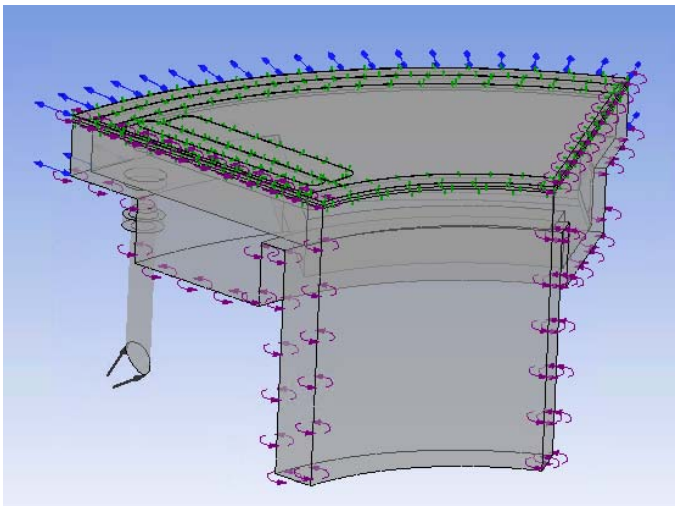

Figure 16: Boundary conditions for the fluid domain of the LEG thrust bearing.

Figure 17 shows the mesh used in the simulation. Axially, four layers are created this time. The film layer is defined as the region between the loaded and runner surfaces, the second is defined by the steel surface in the leading-edge strip and the film layer, the third is defined by the lip at the pad OD and the second layer, and the fourth is the remainder of the fluid (see Fig. 17). The three top layers are meshed using the "sweep" method in the axial direction. The constraints of the sweep method force us to divide each layer into five regions: one defined by the loaded surface, a second defined by the fluid exterior of the pad body, the third defined by the taper, the fourth defined by the groove, and the fifth defined by the leading-edge-strip. Grid refinements in the radial and circumferential directions are as before.

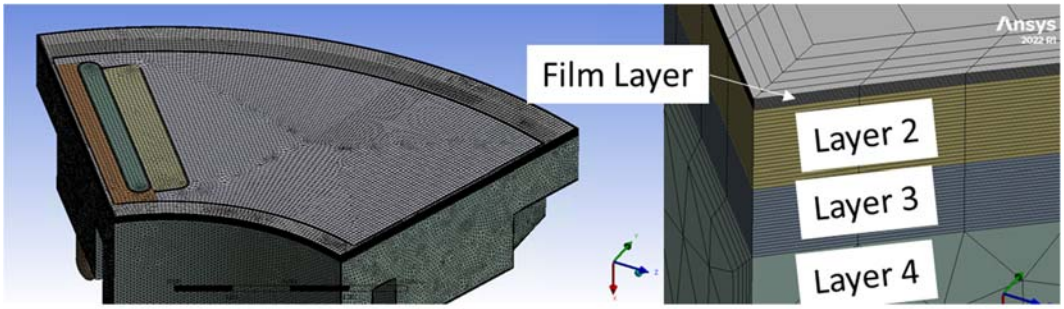

Figure 17: View of the mesh of the fluid domain of the LEG bearing.

Figure 13(b) shows the pressure field induced by the collar rotation. Figure 18 shows the streamlines that are seeded in the film layer at the trailing edge of the region over the loaded surface. First and foremost, the cooling effect of the LEG is clearly seen. Oil in the film layer rapidly cools as it traverses over the groove. That cooling effect become less dramatic over the groove when viewed radially from OD to ID, corresponding to the supply oil in the groove being heated. Note that this is only fluid that it in the uppermost film layer. Figure 19 shows streamlines that originate at the interfaces of layers 2 and 3 (left figure) and layers 3 and 4 (right figure). The noteworthy conclusion from the left figure is that oil does enter the film layer. This oil is not at supply temperature, but it probably helps mitigate heat generated by shear in the oil. The right figure shows that the oil deeper in the bearing that generally does not enter the film.

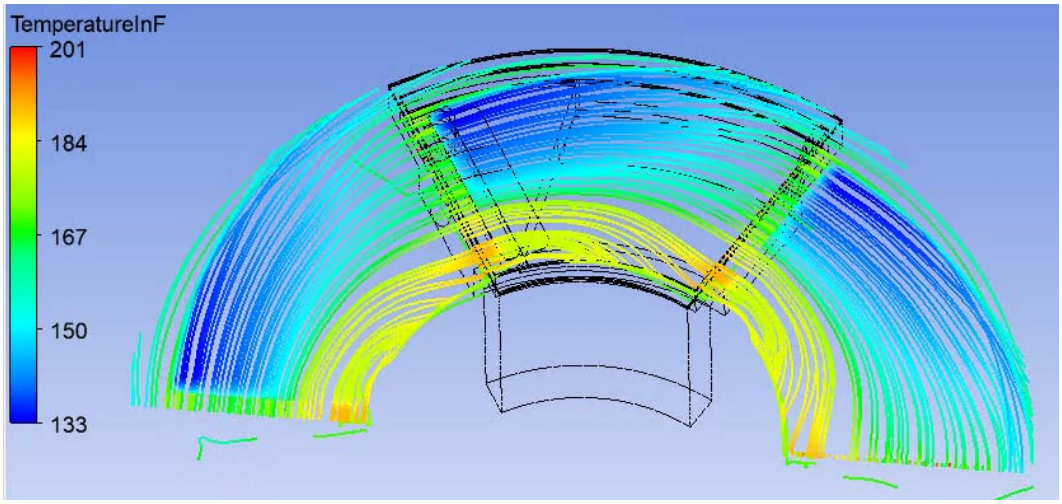

Figure 18: Streamlines for the LEG bearing seeded in the film at the trailing edge of the pad region. The pattern has been repeated to get a better grasp of the streamlines. Shaft rotation is clockwise.

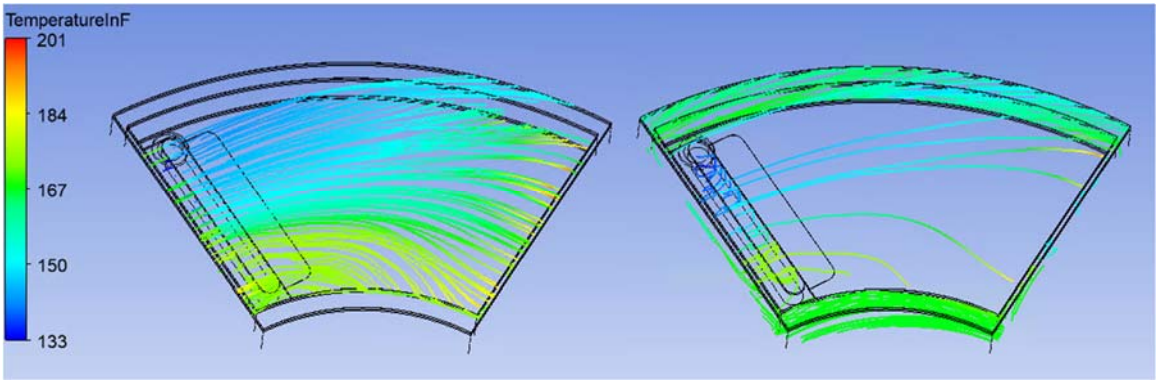

Figure 19: Streamlines for the LEG bearing seeded at the interface of the film and second layers in the groove and tapered regions (left) and at the interface of the third and second regions (right) (refer to Fig. 17). Shaft rotation is clockwise.

Figure 20 shows a close up of the feed groove in the LEG thrust bearing just as the flow exists the feed path in the base ring and enters the groove in the shoe. Clearly seen is the reciruclation zone in the groove. A careful study of this zone shows a trend of cooler oil cooler towards the bottom of the groove and warmer oil towards the top.

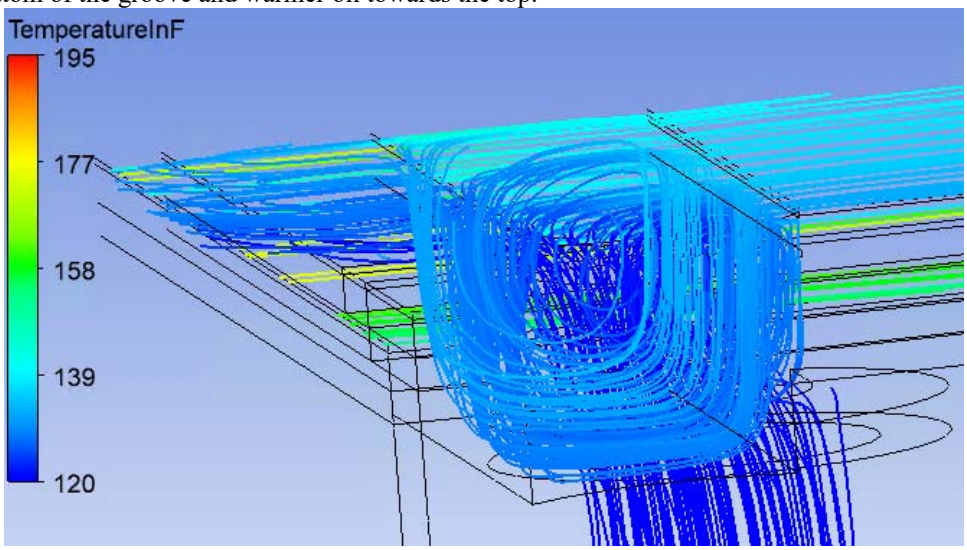

Figure 20: Streamlines for the LEG bearing in the groove at the leading edge of the pad. These streamlines are seeded at the oil supply orifice in the base ring. The dark blue lines are streamlines of cool oil coming from the oil supply. Shaft rotation is clockwise.

Design 3: BPG Bearing

The BPG bearing, the right bearing in Fig. 10, is drastically different from the LEG and flooded bearings. The visible part of the pad in Fig. 10 is a solid pie-shaped body. It is attached to a plate that keeps it from falling out of the base ring (see Fig. 21). Together, these two parts sit on a shoe support located in the upper leveling plate.

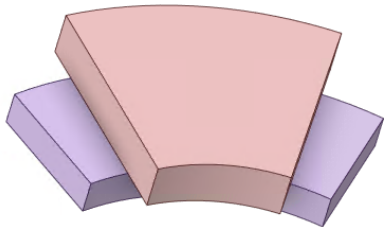

Figure 21: BPG thrust shoe: on the left is the shoe top and bottom.

The boundary conditions for the BPG simulation are almost identical to those for the LEG simulation (see Fig. 16). Figure 22 shows the mesh used in the BPG simulations. We create the $1/6^{th}$ sub-model by cutting the domain using the leading edge of the trough, a fixed datum. Axially, the mesh is divided into three layers: the film layer is defined by the loaded and runner surfaces, the second defined by the top of the BPG trough and the film layer, and the third by the rest of the fluid. Referring to Fig. 22, the film layer is subdivided into four regions: one defined by the loaded surface (orange), the second defined by the edge of the body carrying the trough (green), the third defined by the edge of the trough (beige), and the fourth defined by the remaining fluid (grey). As above, the first two layers are meshed using the "sweep" method in the axial direction. Grid refinement in the radial and circumferential directions is as before.

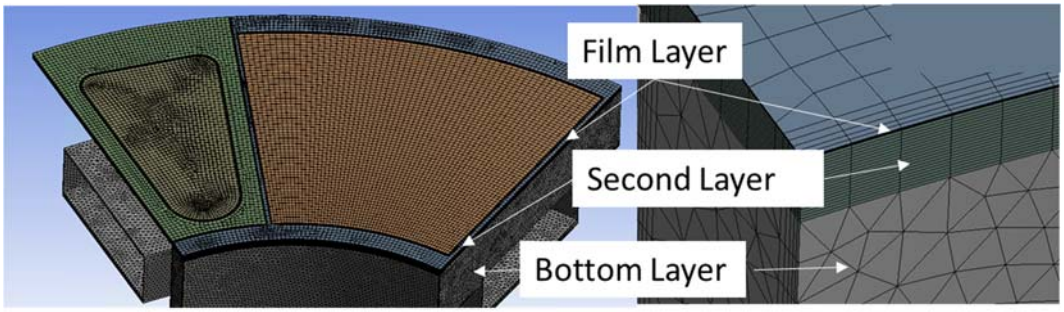

Figure 22: View of the mesh for the fluid domain of the BPG bearing.

Figure 14(c) shows the generated pressure field. Like Figs. 14 and 18, the streamlines in Fig. 23 are seeded at the trailing edge of a loaded region. The distinct cooling mechanism of the BPG is clearly seen. Figure 24 shows the streamlines seeded between the film and second layers above the trough region (left) and at the surface of the trough (right). Cool oil is flows out of the trough and into layer 2, the layer below the film layer. That oil is heated in the short distance from where it enters the region to where it hits the pad, which acts like a dam.

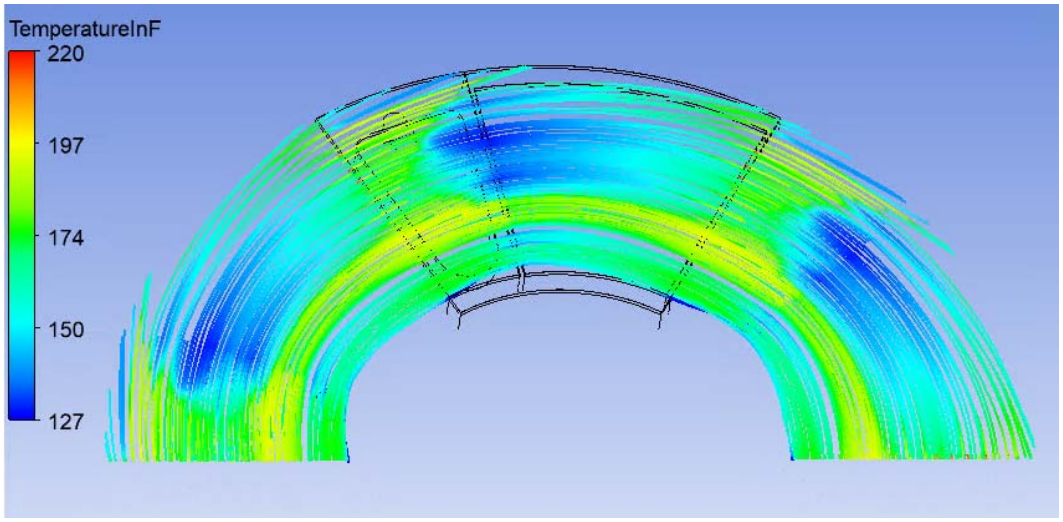

Figure 23: Streamlines for the BPG seeded at the trailing edge of the loaded region. Shaft rotation is clockwise.

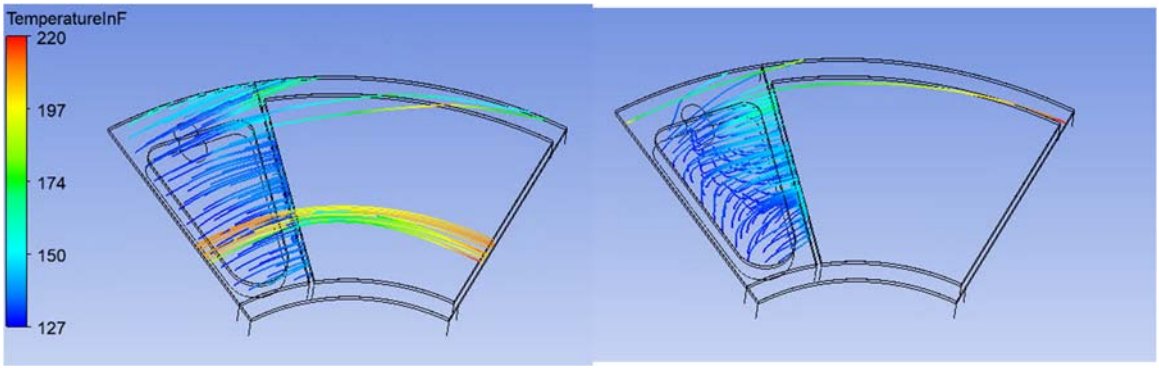

Figure 24: Streamlines for the BPG seeded at the interface of the second and film layers (left) and the third and second layers (right). Shaft rotation is clockwise.

Using HOC factors in Reynolds-equation based solvers

We compare the output of the program THRUST (Brockett, et al. 1996) version 5.4 from the Rotating Machinery and Controls Industrial Program (ROMAC) at the University of Virginia against the test data presented in this paper. The program is a Reynolds-equation-based TEHD finite element solver that analyzes thrust bearing performance. The particular feature of this program that is of interest to this study is that the code allows the user to specify a HOC factor. The model used in this program is based on the model by Mitsui, et al. (1983):

$$T_{LE} = \left(\frac{\lambda Q_{TE}}{Q_{LE}}\right) T_{TE} + \left(1 - \frac{\lambda Q_{TE}}{Q_{LE}}\right) T_S$$

where T is a temperature, Q is oil flow computed from the solution of Reynolds equation, the subscripts TE, LE refer to trailing and leading edges of successive pads, respectively, and the subscript S refers to the oil in the groove between pads. The dimensionless factor λ is the HOC factor. The physical interpretation of the HOC factor is that it is the fraction of heat advected from the trailing edge of one pad to the leading edge of the next pad. When $\lambda = 0$, the exit flow is blocked; and when $\lambda = 1$, there is perfect mixing of the exit and groove flows in the sense that enthalpy is conserved. In a flooded design, one expects $\lambda \approx 1$ since the little mixing occurs between the pads (Fig. 14); in a directed-lubrication bearing, one expects lower values of λ would closely resemble reality (Figs. 18, 24). San Andrés and Abdollahi (2018) proposed a new mixing model which includes the thermal energy from side and churning fluid flows as well as heat convected from pad surfaces into the lubricant. We emphasize that the only option this TEHD program offers to distinguish a directed-lubrication bearing from a flooded bearing is the HOC factor.

The simulations here are meant to show the challenge of using HOC theory with directed-lubrication bearing designs rather than a be a calibration of the code itself. The TEHD program cannot model the undercuts at the leading and trailing edges of the 65% offset bearings considered here (Fig. 10) nor can it model the geometry of a BPG thrust pad in Fig. 21. Consequently, we anticipate some variation between predictions and experimental results. The simulations allow for both thermal and mechanical distortion of the pads. The operating conditions are the same as those given in Table 3 with the exception that the load is not fixed.

Design 1: Flooded

Figure 25 shows the predicted 75/75 temperature by the TEHD program for several values of HOC when run with a 19.2 gpm (76.7 l/min) oil supply flow. We see that the program underpredicts the test data for the low-load case, but it does reasonably well at the other two loads when using the extreme HOC factor value. This agrees with the heuristic argument above and the CFD simulations in the previous subsection—hot and cold oils do not mix efficiently in a flooded bearing.

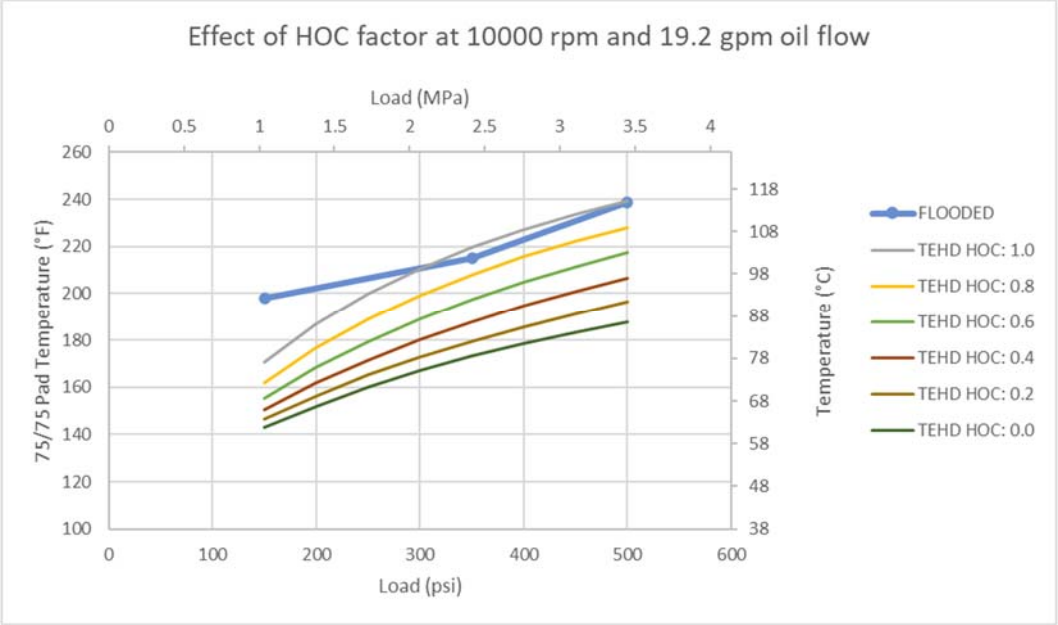

Figure 25: TEHD simulations and flooded test data overlaid for a suite of HOC factors.

Design 2: LEG

Figure 26 shows the predicted 75/75 temperature by the TEHD program for several values of HOC with 17.5 gpm (66.2 l/min) oil supply. These values are only marginally different from those in Fig. 27—the geometry is the same, only the oil supply flow rate is different. That is to say, the groove geometry is to be ignored when setting up the inputs for the TEHD program. Again, the program underpredicts the test data for the low-load case, but it does reasonably well at the other two loads when using a slightly lower HOC factor value than in the flooded bearing. Note that the HOC theory assumes that the entire leading edge is of uniform temperature, and that is not the case from CFD simulations. Hagemann and Schwarze (2018) point out that T_{LE} represents a mean value of the two-dimensional temperature distribution at the leading edge of the pad. They studied the HOC model for LEG journal bearings and proposed a modification that worked with moderate success. In a second analysis, they apply their HOC model on a node-by-node basis, again with mixed success.

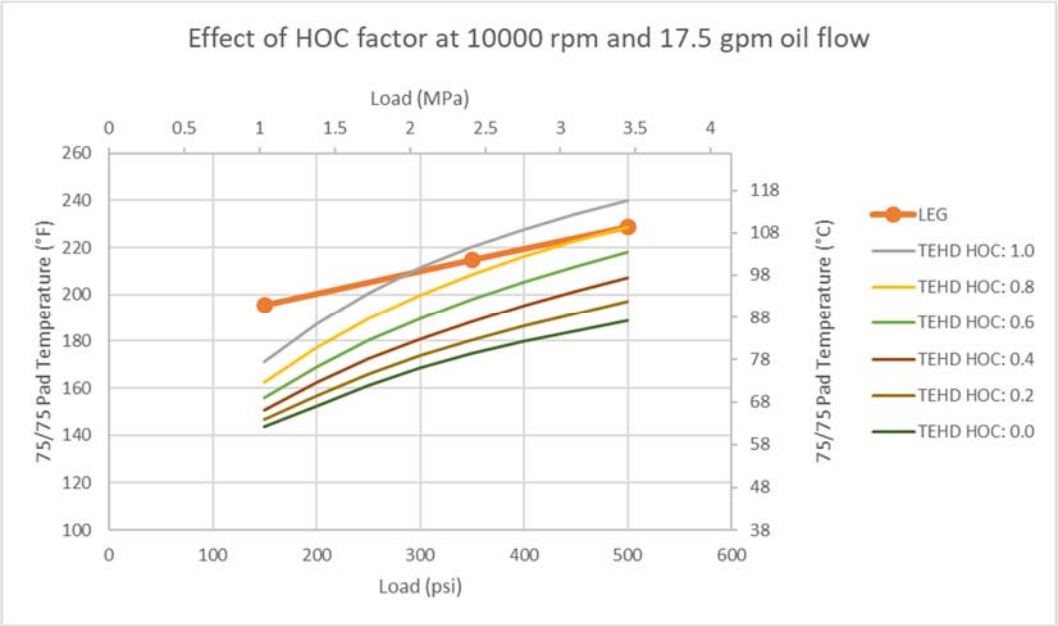

Figure 26: TEHD simulations and LEG test data overlaid for a suite of HOC factors.

Design 3: BPG

The TEHD program has difficulty simulating the BGP thrust bearing. The BPG shoe in Fig. 21 cannot be modeled directly for reasons different from the other designs. The program converges to a solution for high loads and most HOC factors, shown as solid lines in Fig. 27. The dashed line for a HOC factor of 1.0 is extrapolated from the converged solutions using a polynomial fit of the data. Curiously, it appears the BPG requires a HOC factor that lies in between that required for the LEG and for the flooded bearings. At 53 kN, this agrees with the data presented in Fig. 7.

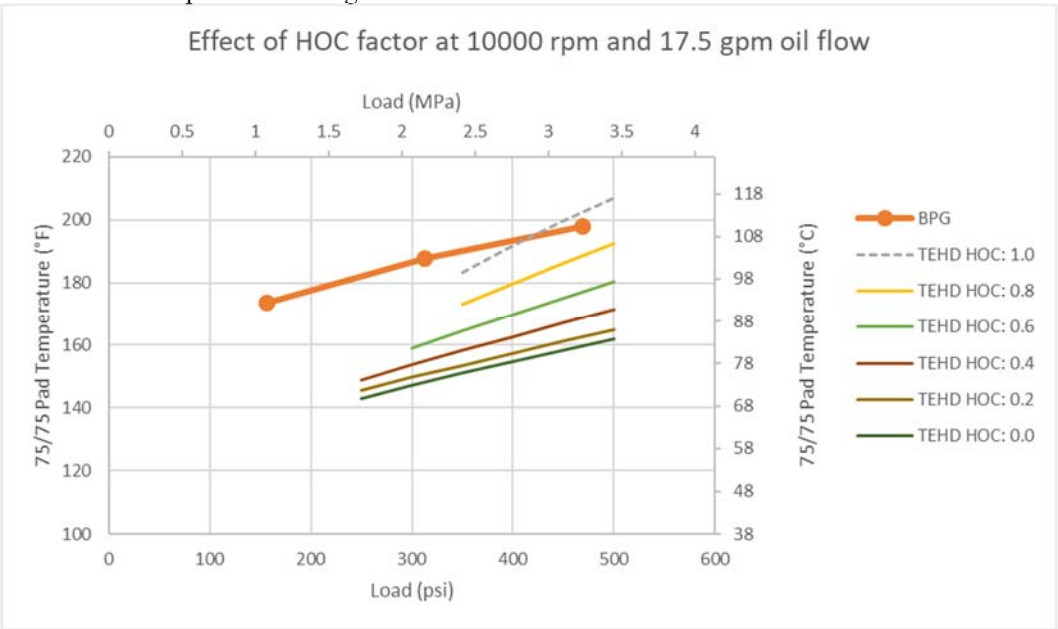

Figure 27: TEHD simulations and BPG test data overlaid for a suite of HOC factors where the program was able to converge. The dashed line is extrapolated from the solid lines.

Discussion

Two conclusions can be drawn from the simulations shown in Figs. 25-27. First, it appears that the HOC factor is a function of bearing load rather than a constant for each bearing type. Second, an HOC factor larger than unity is needed to match test results for low loads. Surprisingly, the TEHD code allows for HOC factors bigger than unity, and simulations for $\lambda > 1$ shown in Fig. 28 for the LEG bearing support this conjecture. Such a value for the HOC factor makes no physical sense in Mitsui's model. Instead, we postulate the following. We mentioned earlier that the TEHD code does not correctly model the undercuts on the leading edge of an offset thrust bearing correctly. In such a case, one could view using HOC values $\lambda > 1$ as a numerical tool to compensate for the TEHD's modeling shortcomings.

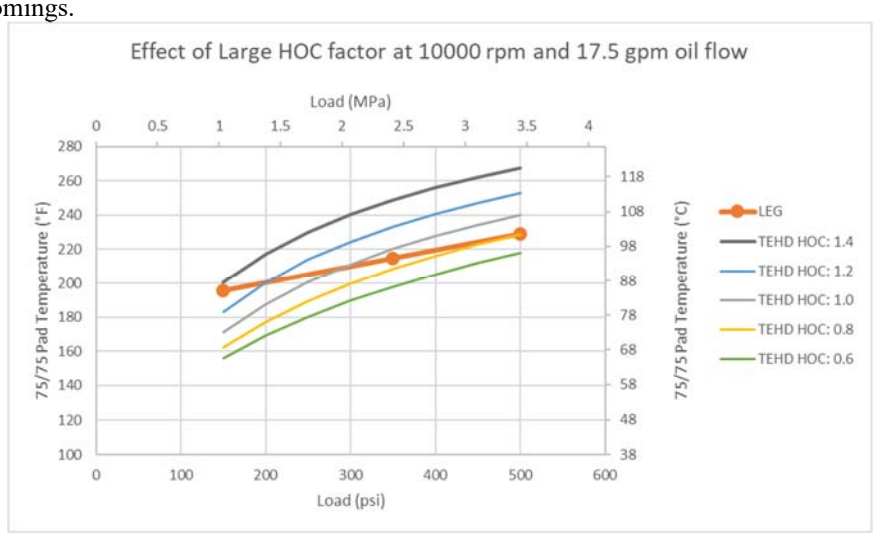

Figure 28: TEHD simulations and LEG test data overlaid for HOC values greater than unity.

CONCLUSIONS

We compare three bearing designs: classical flooded, LEG, and BPG. The comparison is on three levels: performance on a test stand, CFD analysis, and TEHD analysis. The three designs are similar in that they are all six-shoe equalizing thrust bearings with the same ID and OD, and they differ in their cooling mechanisms.

We show that the BPG design outperforms the other two designs on a test stand when keeping in mind that the bearing area of the BPG is lower than that of the flooded and LEG designs. The implication is that the BPG meets the small-footprint demand of modern applications, and we present an example where this is the case.

Our idealized CFD simulations on the three different cooling mechanisms demonstrate that the flow pattern in each bearing design is unique. The flooded bearing clearly has the worst heat performance. And the stark contrast between the LEG and the BPG is clearly shown—the LEG bleeds cool oil into the film whereas the BPG appears to rely on oil mixing in and over the trough. Future work will include heat conduction to the solids as well as deflection of the solids followed by a detailed study of these bearings over a large range of speeds, loads, and flows.

Finally, we demonstrate the difficulty in using Mitsui's HOC theory as coded in a TEHD program to model these directed-lubrication bearings in a Reynolds-equation based solver. In the case of the BPG, the solver was unable to converge for a number of cases. For low loads, we show that using an HOC factor larger than unity, though unphysical, helps match test data. Although we had hoped that the HOC factor is a constant for each bearing type, it appears to a function of load at least.

NOMENCLATURE

T	= Temperature	(T)
Q	= Flow	(V/t)
λ	= Hot Oil Carryover Factor	(-)
LEG	= Leading Edge Groove	
BPG	= Between Pad Groove	
HOC	= Hot Oil Carryover	
CFD	= Computational Fluid Dynamics	
OD	= Outer Diameter	
ID	= Inner Diameter	

APPENDIX A

Table 1 shows that the flooded bearings were tested at speeds different from the other campaigns. The solid lines in Fig. 33 shows the raw data from that test. We interpolate the data for each load as a function of speed using simple cubic curve fits. The interpolated data appear as green dashed lines in Fig. 32. It is this interpolated data that we use in throughout the paper.

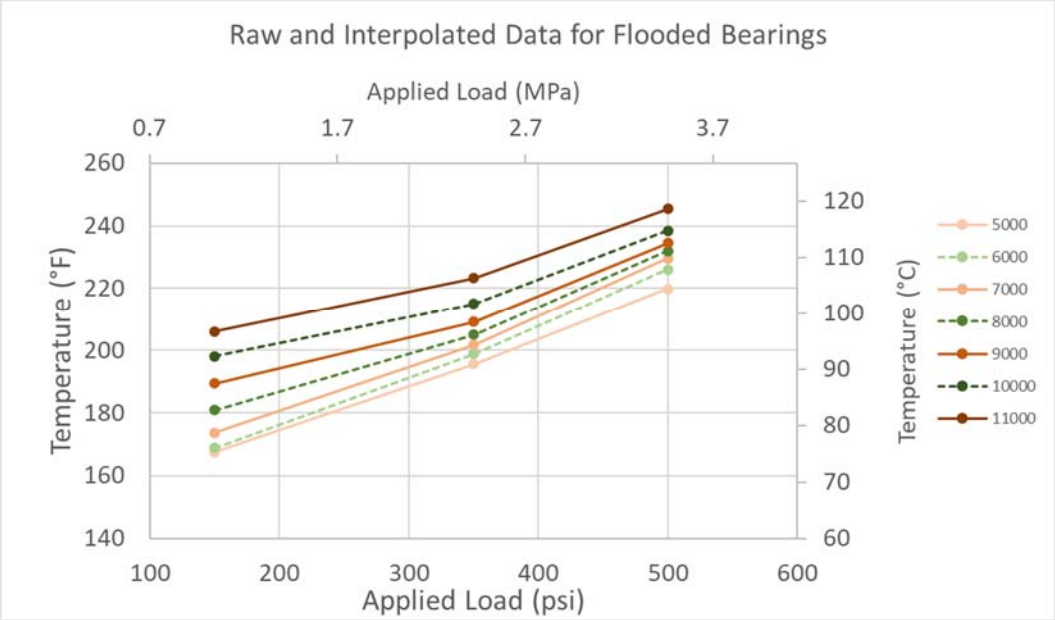

Figure 29: Plots of actual and interpolated test data for the flooded bearing.

The flow rates in Table 1 follow a linear trend. The flow rate for 10,000 rpm is 19.2 gpm.

REFERENCES

Ball, J. H., 1996, "Design Considerations for Trust Bearing Applications," *Proceedings of the 25th Turbomachinery Symposium*, Turbomachinery Laboratory, Texas A&M University, College Station, Texas, pp. 223-242.

Ball, J. H. and Byrne, T. R., 1999, "Tilt Pad Hydrodynamic Bearing for Rotation Machinery," US Patent No. 5,879,085.

Ball, J. H. and Gardner, W. W., 1991, "Method of Making a Low Flow Tilting Pad Thrust Bearing," US Patent No. 5,068,965.

Bolton, I.E., 1926, "Improvements in Film Lubricated Thrust Bearings," GB Patent No. 263,378.

Brockett, T. S., Barrett, L. E., and Allaire, P. E., 1996, "Thermoelastohydrodynamic analysis of fixed geometry thrust bearings including runner deformation," Trib. Trans., 39, pp. 555–562.

Brockwell, K., Dmochowski, W., and DeCamillo, S., 1994, "Analysis and Testing of the LEG Tilting Pad Journal Bearing—A New Design for Increasing Load Capacity, Reducing Operating Temperatures and Conserving Energy," *Proceedings of the 23rd Turbomachinery Symposium,* Turbomachinery Laboratory, Texas A&M University, College Station, Texas, pp. 43-56.

Capitao, J. W., Gregory, R. S., and Whitford, R. P., 1976, "Effects of High-Operating Speeds on Tilting Pad Thrust Bearing Performance," J. Lub. Tech., 98, pp. 73-80.

Capitao, J.W., 1976, "Performance Characteristics of Tilting Pad Thrust Bearings at High Operating Speeds," J. Lub. Tech., 98, pp. 81-89.

DeCamillo, S., 2005. Personal Archives at Kingsbury, Inc.

DeCamillo, S. and Fabijonas, B.R., 2012, "Chapter 45: Thrust Bearings," *Handbook of Lubrication and Technology, Vol. 2*, R.W. Bruce ed., CRC Press, Boca Raton, FL, 21pp.

Edney, S.L., Heitland, G.B. and DeCamillo, S.M., 1998, "Testing, Analysis, and CFD Modeling of a Profiled Leading Edge Groove Tilting Pad Journal Bearing," *Proceedings of the International Gas Turbine & Aeroengine Congress & Exhibition*, 98-GT-409, 9pp.

Firth, R.V., 1933, "Oil Device for Bearings," US Patent No. 1,900,924.

Gates, H., 2019, “Review of Thermal Mixing Models,” ROMAC Annual Meeting 2019.

Gregory, R. S., 1974, “Performance of Thrust Bearings at High Operating Speeds,” Trans. ASME/J. Lub. Tech., 96, pp. 7-14.21

Gregory, R. S., 1977, “Operating Characteristics of Fluid-Film Thrust Bearings Subjected to High Shaft Speeds,” *Super Laminar Flow in Bearings: Proceedings of the Second Leeds-Lyon Symposium on Tribology*, Dowson, Godet, and Taylor eds., Mech. Eng. Pub. Ltd, London, pp. 154-155.

Gregory, R. S., 1979, “Factors Influencing Power Loss of Tilting-Pad Thrust Bearings,” Trans ASME/J. Lub. Tech., 101, pp. 154-163.

Gregory, R. S., 1985. “Thrust Bearing,” US Patent No. 4,501,505.

Hagemann, T. and Schwarze, H., 2018, “Theoretical and Experimental Analyses of Directly Lubricated Tilting-Pad Journal Bearings with Leading Edge Groove,” *Proceedings of the ASME Turbo Expo 2018*, GT2018-75659, 12pp.

He, M., 2003, “Thermoelastohydrodynamic Analysis of Fluid-Film Journal Bearings,” *Ph.D. Dissertation*, University of Virginia, Charlottesville, VA.

Hübner, B. and Silva, D.R.B., 2019, “Advanced simulation of coupled physics in thrust bearings,” *IOP Conf. Ser.: Earth Environ. Sci.,* 240, 062009, 7pp.

Koosha, R. and San Andrés, L., 2020, “A Computational Model for the Analysis of the Static Forced Performance of Self-Equalizing Tilting Pad Thrust Bearings,” *Proceedings of the ASME Turbo Expo 2020*, GT2020-16060, 13pp.

Lakey, A. B., 1950, “Thrust Bearing,” US Patent No. 2,507,021.

Mikula, A. M. and Gregory, R. S., 1983, “A Comparison of Tilting-Pad Thrust Bearing Supply Methods,” Trans. ASME/J. Tribology, 105, pp. 39-47.

Mikula, A. M., 1985, “The Leading Edge Groove Tilting Pad Thrust Bearing: Recent Developments,” Trans. ASME/J. Tribology, 107, pp. 423-430.

Mikula, A. M., 1986, “Evaluating Tilting Pad Thrust Bearing Operating Temperatures,” Trans. ASLE, 29, pp. 173-178.

Mikula, A. M., 1988a, “Further Test Results of the Leading Edge Groove (LEG) Tilting Pad Thrust Bearings,” Trans. ASME, 110, pp. 174-180.

Mikula, A. M., 1988b, “The Effet of Shoe Backing Material on the Thermal Performance of a Tilting-Pad Thrust Bearing,” J. Soc. Tribologists & Lub. Engrs, 44, pp. 969-973.

Mitsui, J., Hori, Y., and Tanaka, M., 1983, “Thermohydrodynamic analysis of cooling effect of supply oil in Circular Journal Bearing,” J. Lub. Tech., 105, pp. 414-420.

Pajączkowski, P., 2010, “Simulation of transient states in large hydrodynamic thrust bearings,” *Ph.D. Dissertation*, Gdańsk University of Technology, Gdansk, Poland.

San Andrés, L. and Abdollahi, B., 2018, “On the Performance of Tilting Pad Bearings: A Novel Model for Lubricant Mixing at Oil Feed Ports wit Improved Estimation of Pads’ Inlet Temperature and Its Validation Against Experimental Data,” *Proceedings of the Asia Turbomachinery And Pump Symposium*, Turbomachinery Laboratory, Texas A&M University, College Station, Texas, 31pp.

San Andrés, L. and Koosha, R., 2018, “A Thermo-Elasto-Hydrodynamic (TEHD) Computational Analysis of Tilting Pad Thrust Bearings: Analytical and FE Pad Structure Models,” *Research Progress Report to the TAMU Turbomachinery Research Consortium*, Turbomachinery Laboratory, Texas A&M University, College Station, Texas, TRC-B&C-01-18:37pp.

Seeton, C.J., 2006, “Viscosity-temperature correlation for liquids,” Trib. Lett., 22, pp. 67-78.

Wilkes, J. J. and DeCamillo, S. M., 2000, “Thrust Bearing,” US Patent No. 6,089,754.

Wilkes, J., DeCamillo, S., Kuzdzal, M., and Mordell, J., 2000, "Evaluation of a High Speed, Light Load Phenomena in Tilting Pad Thrust Bearings," *Proceedings of the 29th Turbomachinery Symposium*, Turbomachinery Laboratory, Texas A&M University, College Station, Texas, pp. 177-185.

Yang, J. and Palazzolo, A., 2019a, "Three-Dimensional Thermo-Elasto-Hydrodynamic Computational Fluid Dynamics Model of a Tilting Pad Journal Bearing—Part I: Static Response," J. Trib., 141, 21pp.

Yang, J. and Palazzolo, A., 2019b, "Three-Dimensional Thermo-Elasto-Hydrodynamic Computational Fluid Dynamics Model of a Tilting Pad Journal Bearing—Part II: Dynamic Response," J. Trib., 141, 16pp.

Yang, J. and Palazzolo, A., 2021a, "Computational Fluid Dynamics Based Mixing Prediction for Tilt Pad Journal Bearing TEHD Modeling—Part I: TEHC-CFD Model Validation and Improvements," J. Trib., 143, 20pp.

Yang, J. and Palazzolo, A., 2021b, "Computational Fluid Dynamics Based Mixing Prediction for Tilt Pad Journal Bearing TEHD Modeling—Part II: Implementation with Machine Learning," J. Trib., 143, 21pp.

Yang, J. and Palazzolo, A., 2022a, "Tilt Pad Bearing Distributed Pad Inlet Temperature with Machine Learning—Part I: Static and Dynamic Characteristics," J. Trib., 144, 20pp.

Yang, J. and Palazzolo, A., 2022b, "Tilt Pad Bearing Distributed Pad Inlet Temperature with Machine Learning—Part II: Morton Effect," J. Trib., 144, 20pp.

ACKNOWLEDGEMENTS

The authors thank Kingsbury, Inc. for encouragement, editorial comments, and permission to publish these results. The authors are forever indebted to their late mentor Scan DeCamillo under whose guidance most of these tests were conducted. The authors also thank the referees whose critical review of early drafts greatly improved the presentation of the material.